Sensors & Transducers, Vol. 247, Issue 8, December 2020, pp. 18-24

Sensors & Transducers
Published by IFSA Publishing, S. L., 2020
http://www.sensorsportal.com

Numerical Analysis of CCD Images for Polarimetry with Full Poincaré Beams

[1, *] Juan C. SUÁREZ-BERMEJO, [2] Juan C. GONZÁLEZ DE SANDE, [3] Massimo SANTARSIERO and [4] Gemma PIQUERO

[1] Universidad Politécnica de Madrid, Materials Science, Av. de la Memoria 4, 28040 Madrid, Spain
[2] Universidad Politécnica de Madrid, ETSIS de Telecomunicación, Campus Sur, 28031 Madrid, Spain
[3] Università Roma Tre, Dipartimento di Ingegneria, V. Volterra 62, Rome 00146, Italy
[2] Universidad Complutense de Madrid, Departamento de Óptica, 28040 Madrid, Spain
[1] Tel.: +34 910 676 214
[*] E-mail: juancarlos.suarez@upm.es

Received: 10 November 2020 /Accepted: 10 December 2020 /Published: 31 December 2020

Abstract: Full Poincaré beams have been recently applied in polarimetry for determining the Mueller matrix of homogeneus samples. Such matrix can be obtained from the measured Stokes parameters at four selected points across the transverse section of a full Poincaré beam before and after the sample. Since the transverse section of a full Poincaré beam contains all the possible states of polarization, the possibility of changing the input polarization state on selecting different points could be exploited to get a better accuracy in the determination of the Mueller matrix. To this aim, a polarization state analyzer with a CCD camera can be used to obtain maps of the Stokes parameters across the transverse section of input and output beams. The analysis of the obtained polarization maps can lead to the determination of the Mueller matrix with reduced uncertainties. Several simulations are presented and compared to show the feasibility of this proposal.

Keywords: Polarization, Polarimetry, Full Poincaré beams, CCD, Error sources.

1. Introduction

The analysis of the changes in polarization pattern of a non-uniformly polarized beam (see Ref. [1] and references therein) has been proposed for Mueller matrix polarimetry [2-15]. Full Poincaré beams (FPBs) are a class of non-uniformly totally polarized beams that present all possible states of totally polarized light across their transverse section [16]. This feature can be exploited in polarimetric applications, where such kind of beams can be used as a parallel polarization state generator (PSG). It has been shown that a particular type of FPB can be easily synthesized by focusing a linearly polarized beam onto a plane parallel slab of uniaxial crystal with its optic axis perpendicular to the slab [17, 18]. For this particular FPB, all possible states of polarization can be found within a semicircle across the beam transverse section, with a given radius r_M, whose value depends on the thickness of the slab and the refractive indexes of the crystal at the working wavelength. By measuring the Stokes parameters at four different points of the transverse section of a FPB before and after a homogeneous sample, the Mueller matrix of the sample can be determined [19, 20].

Here, we propose the use of a CCD camera instead of a point-like detector to measure the Stokes parameters in the whole section of the FPB. Then, many sets of four pixels can be used to obtain the Mueller matrix of the sample. Simulations of the measurement process show the potential improvement that could be achieved by averaging the results on a large number of combinations of measurement points.

In the following section, the method to simulate the polarimetric measurement process using a FPB and a CCD camera will be outlined. Then, the analysis of the errors due to the inaccuracy of the intensity measurement of the CCD camera will be studied and the results of the simulations will be presented in Section 3. Finally, the main conclusions of this work will be presented in Section 4.

2. Simulation of a Polarimetric Measurement with a FPB and a CCD Camera

Stokes vector at a given point in the transverse section of a light beam, $\vec{S}^{in}$, can be obtained by measuring the light intensity in such a point after a linear polarizer (P) with its transmission axis oriented at four different angles, namely, $0°, 45°, 90°, 135°$ (denoted as I_0, I_{45}, I_{90}, I_{135}, respectively); and after the combination of a quarter wave plate (QWP) and the linear polarizer oriented at 45°, 135° (denoted by $I_{QWP,45}$ and $I_{QWP,135}$) [2, 3]. This system constitutes a polarization state analyzer (PSA). By recording the intensity with a camera, a map of the Stokes parameters can be obtained. If the same light beam passes through a given sample, represented by a 4×4 Mueller matrix, $\widehat{M}$, the state of polarization changes depending on the sample characteristics as

$$\vec{S}^{out} = \widehat{M}\vec{S}^{in}, \tag{1}$$

where $\vec{S}^{out}$ is the Stokes vector of the output beam.

By measuring the Stokes parameters of the output beam for at least four different states of polarization of the input beam the Mueller matrix of the sample can be recovered. When the input beam is a FPB, and the Stokes parameters are measured in its transverse section with a CCD camera before and after the sample, many combinations of four different pixels can be used to determine the Mueller matrix of the sample. The experimental setup is shown in Fig. 1.

Considering optical elements (polarizer and quarter wave plate) that are ideal and perfectly oriented, an important source of error is the inaccuracy in the measurement of the light intensity at each pixel of the acquired images [5, 9, 12]. In order to evaluate this source of error, the intensity maps that would be obtained when the considered FPB passes through the PSA for six different configurations (I_0, I_{90}, I_{45}, I_{-45}, $I_{45,QWP}$, $I_{45,QWP}$) are theoretically calculated (see Fig. 1.b). Then, a random Gaussian noise is added to each of these calculated images (AGN, Fig. 1.c). From these noisy images, the maps of Stokes parameters for the input beam are calculated (Fig. 1.d). The same procedure is followed when a sample (with a known Mueller matrix $\widehat{M_T}$) is inserted before the PSA (Figs. 1.e-h). Finally, from the input and output Stokes parameter maps, the Mueller matrix of the sample, $\widehat{M_S}$, is evaluated. This simulation process have been repeated N_s=5 times and the average of the final results has been taken.

The Stokes vector of the beam at any point (r, θ) of the beam section at the exit of a uniaxial crystal illuminated with a divergent beam (see Fig. 1.a) can be approximated by [19, 20]

$$\vec{S}(r,\theta) = S_0(r,\theta) \times \begin{bmatrix} 1 \\ -[\cos^2 2\theta + \sin^2 2\theta \cos\delta(r)] \\ -\sin 2\theta \cos 2\theta [1 - \cos\delta(r)] \\ \sin 2\theta \sin\delta(r) \end{bmatrix}, \tag{2}$$

being $\delta(r)$ a phase given by

$$\delta(r) = k(n_e - n_o)\frac{r^2}{l}, \tag{3}$$

where k is the vacuum wave number, l is the crystal length, and n_o and n_e are the ordinary and extraordinary refractive indexes of the uniaxial crystal, respectively.

It has been shown that for this particular beam, all possible totally polarized states of polarization can be found across the beam section inside a semicircle with radius

$$r_M = \sqrt{\frac{\pi l}{k|n_e - n_o|}} \tag{4}$$

A possible way to recover the Mueller matrix consists in using the Stokes vector values at four different pixels (the same set for the input and output maps). The selected pixels must be chosen in such a way that the four corresponding input Stokes vectors be linearly independent (we recall that the coordinates of a point across the beam transverse section presenting a specific state of polarization can be obtained using specific analytical expressions [19, 20]). The optimum choice of the input states of polarization is such that they form a regular tetrahedron inscribed in the Poincaré sphere (see Fig. 2.a) [9]. The corresponding polarization states are found at the locations shown in Fig. 2.b [19, 20].

A continuous rotation of the tetrahedron around the s_1 axis yields a movement of the three points out of the center along the green ovoids in Fig. 2.b. The recovered Mueller matrix can be found on repeating the inversion of Eq. (1) for many sets of the four selected pixels, and averaging the results. The differences between the elements of the obtained Mueller matrix and those of the original one will be evaluated.

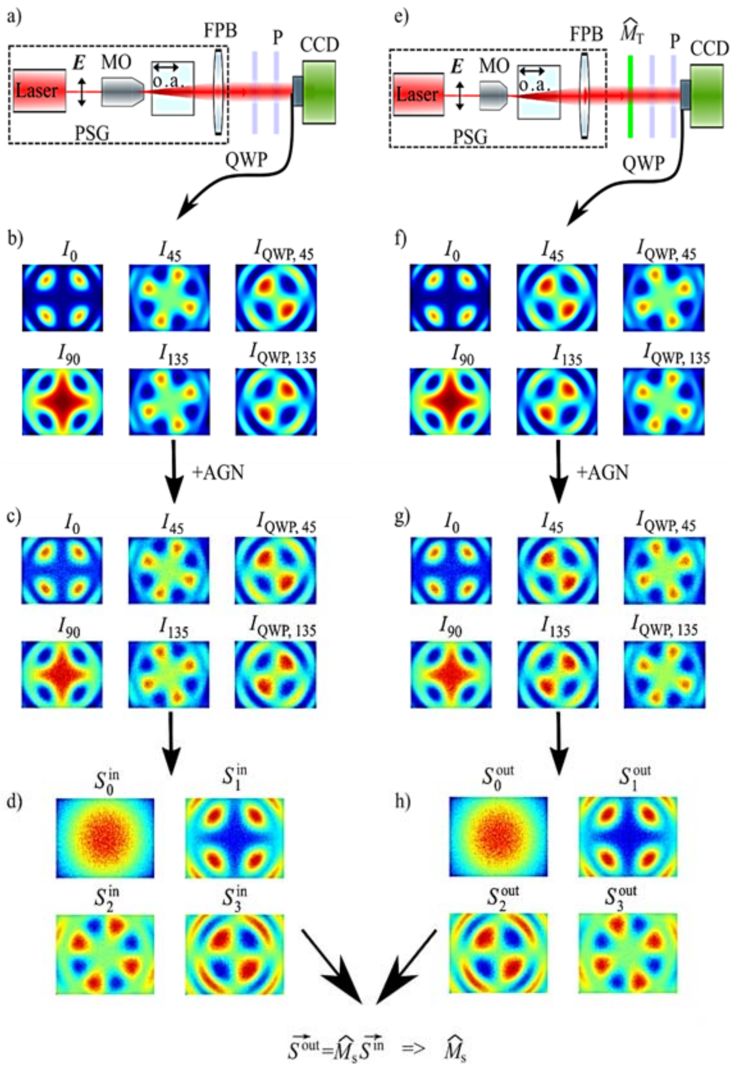

Fig. 1. Scheme of Mueller matrix determination using a Full Poincaré beam and a CCD camera. a) Parallel polarization state generator (PSG) by means of a specific FPB and polarimetric characterization through a PSA; b) theoretical images for six specific configurations of the PSA; c) the same images as in b) with added Gaussian noise (AGN); d) noisy Stokes parameter maps for the FPB; e) polarimetric characterization of the generated FPB after passing through a sample represented by a Mueller matrix $\widehat{M_T}$; f) theoretical images for six configurations of the PSA; g) the same images as in f) with AGN; h) noisy Stokes parameter maps for the output beam.

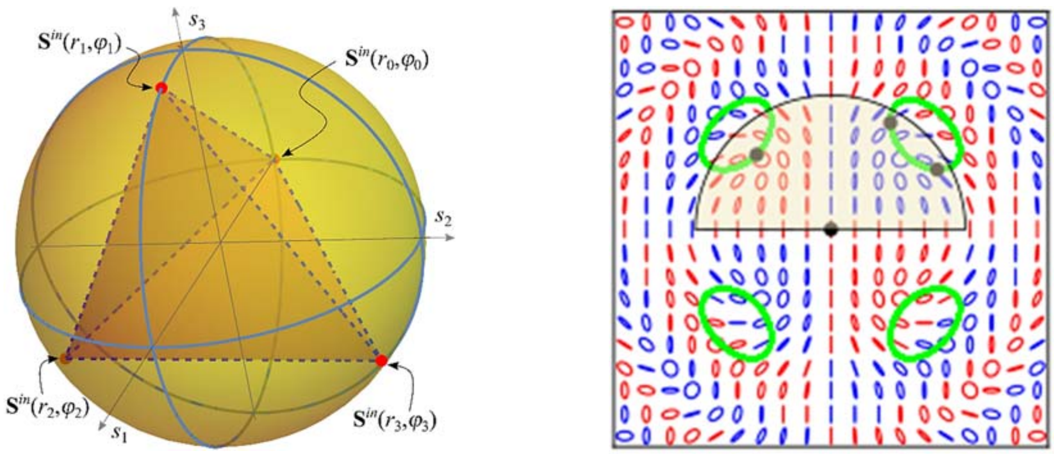

(a) (b)

Fig. 2. a) Poincaré sphere with a set of optimum polarization states for polarimetric measurements. b) Polarization map across the beam section and points where the polarization states represented in a) are found. Red (blue) ellipses represent right-handed (left-handed) polarization states. The semicircle has radius r_M given in Eq. (4). All possible polarization states are found in this semicircle.

3. Error Analysis

To obtain a quantitative estimate of the errors in the determination of Mueller matrix for a considered sample, two different strategies have been followed. In first place, the four pixels that include the theoretical points where the polarization states represented in Fig. 2a are chosen. Note that the state with the following Stokes vector

$$\vec{S}^{in}(r_0, \varphi_0) = [1, -1, 0, 0]^T, \qquad (5)$$

which can be found at the FPB axis, is always taken because the intensity is maximum there. Several sets of the three remaining points across the transverse plane of the beam have been selected in such a way that their polarization states correspond to rotations of the tetrahedron inscribed in the Poincaré sphere around the axis s_1 (see Fig. 2) [9, 18-20]. Due to its symmetry, the rotation of the tetrahedron can be limited to the interval $\left[-\frac{\pi}{6}, \frac{\pi}{6}\right)$. The coordinates of the four considered points are mapped on the CCD images (red pixels in Fig. 3, for one of the choices), both for the input beam (without the sample, with added Gaussian noise), and for the output beam (after passing through the sample, and with a different pattern of added Gaussian noise). Theoretical matrix for every ideal sample is compared to the matrix obtained from simulations and the differences are derived for every element of $\widehat{M}$. An average estimate of the error is obtained from 15 analyzed sets, and the uncertainties of these values are computed. We shall refer to this first approach of Mueller matrix determination as the *center points* strategy.

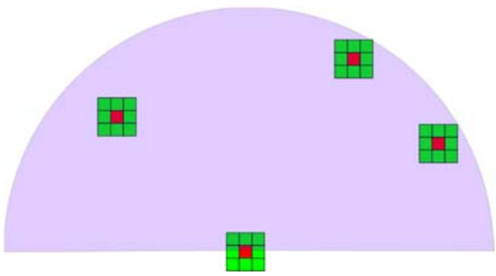

Fig. 3. Red squares represent pixels that contain the point where the ideal FPB presents the states of polarization corresponding to the vertexes of the tetrahedron of Fig. 1a. They are the ones used for the center points strategy. Green squares together the center one represent the 3x3 nearest neighbors. Any combination of four of these pixels around the red ones is used for the nearest neighbors strategy. Shaded semicircle represents a possible area of the beam cross section where all possible states of polarization are found.

The second strategy uses a wider set of points, all located around each of the center points considered in the previous case. A total of NxN nearest neighbor pixels are considered around every center point (see Fig. 3). Mueller matrices are obtained for all the possible four-point sets (input and output) that can be chosen from the N^2x4 pixels included in the analysis. That means a total of $(N^2)^4$ possible combinations. For all of them, the condition number for the equation system formed by evaluating Eq. (1) at four different locations is computed and the resulting Mueller matrix is discarded if such condition number is over 20. An average value is then computed from all the valid cases, for the 15 analysed orientations of the tetrahedron in the Poincaré sphere. We shall refer to this second approach of Mueller matrix determination as the *nearest neighbors* strategy.

Mueller matrices are obtained from the simulated Stokes input and output vectors for four different standard samples: air, a linear polarizer with horizontal transmission axis (LP0) and with its transmission axis at 60º with respect to the horizontal (LP60), and a quarter wave phase (QWP) retarder with its fast axis along the horizontal direction.

Fig. 4 shows the root mean squared value of the difference between the mean matrix obtained for the *Ns* simulations at each orientation of the tetrahedron and the theoretical one, $rms\left(\langle\widehat{M_S}\rangle - \widehat{M_T}\right)$, for each of the four samples considered. This value is calculated as

$$rms\left(\langle\widehat{M_S}\rangle - \widehat{M_T}\right) = \frac{1}{4}\sqrt{\sum_{i,j=0}^{3}\left(\overline{m}_{ij}^S - m_{ij}^T\right)^2}, \qquad (6)$$

where $\overline{m}_{ij}^S$ are the mean values of the Mueller matrix elements obtained from the simulation and m_{ij}^T are the theoretical ones.

For these simulations a Gaussian noise with amplitude $\varepsilon = 0.01$ of the maximum intensity of the beam has been added to each pixel of the images in Fig. 1.b and Fig. 1.f. The results for both the center points and nearest neighbors strategies are presented. In all the cases, the nearest neighbor strategy renders a smaller value of the error compared to the center points strategy. It is worth noting that the orientation of the tetrahedron around the s_1 axis has no influence on the obtained results.

The results for the simulations with a Gaussian noise amplitude $\varepsilon = 0.02$ are shown in Fig. 5. It can be observed that the root mean squared values of the difference between the theoretical Mueller matrix and the one obtained from the simulations, almost double the corresponding ones in Fig. 4. However, differences can be observed for different samples considered in the analysis. For example, the linear polarizer with its axis along the horizontal direction shows better results than the other three samples, for which the rms of the differences between the simulated measurements and the theoretical Mueller matrices are similar.

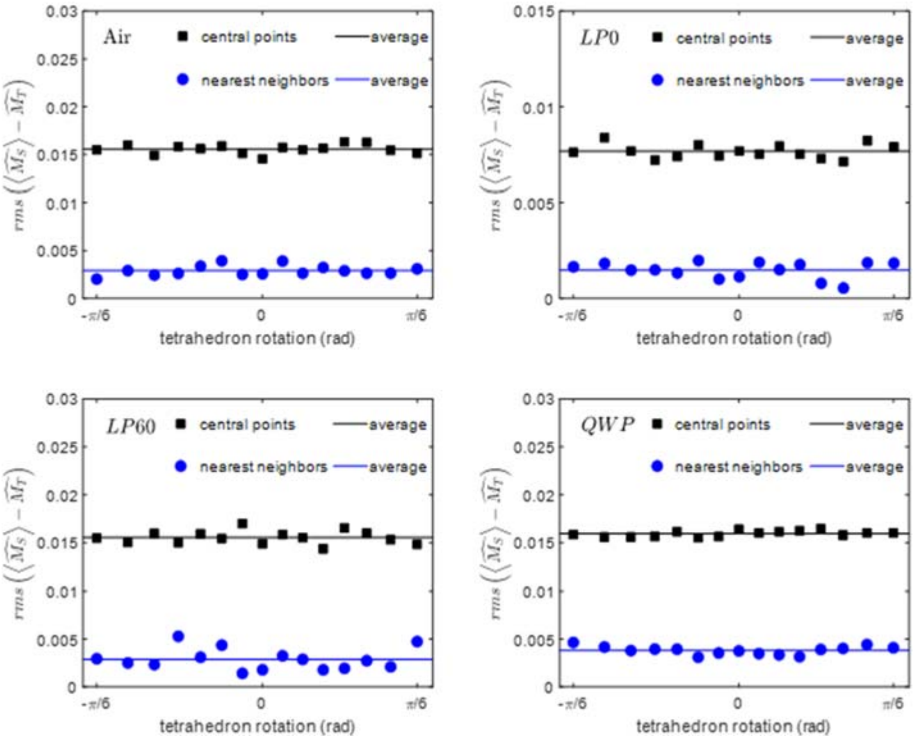

Fig. 4. Individual and mean values of the rms of differences between the Mueller matrix obtained from numerical simulation and theoretical ones, for four different ideal samples, assuming a maximum amplitude of Gaussian noise of $\varepsilon = 0.01$. The four samples are air, a linear polarizer with horizontal transmission axis (LP0) and with its transmission axis at 60° with respect to the horizontal (LP60), and a quarter wave phase (QWP) retarder with its fast axis along the horizontal direction.

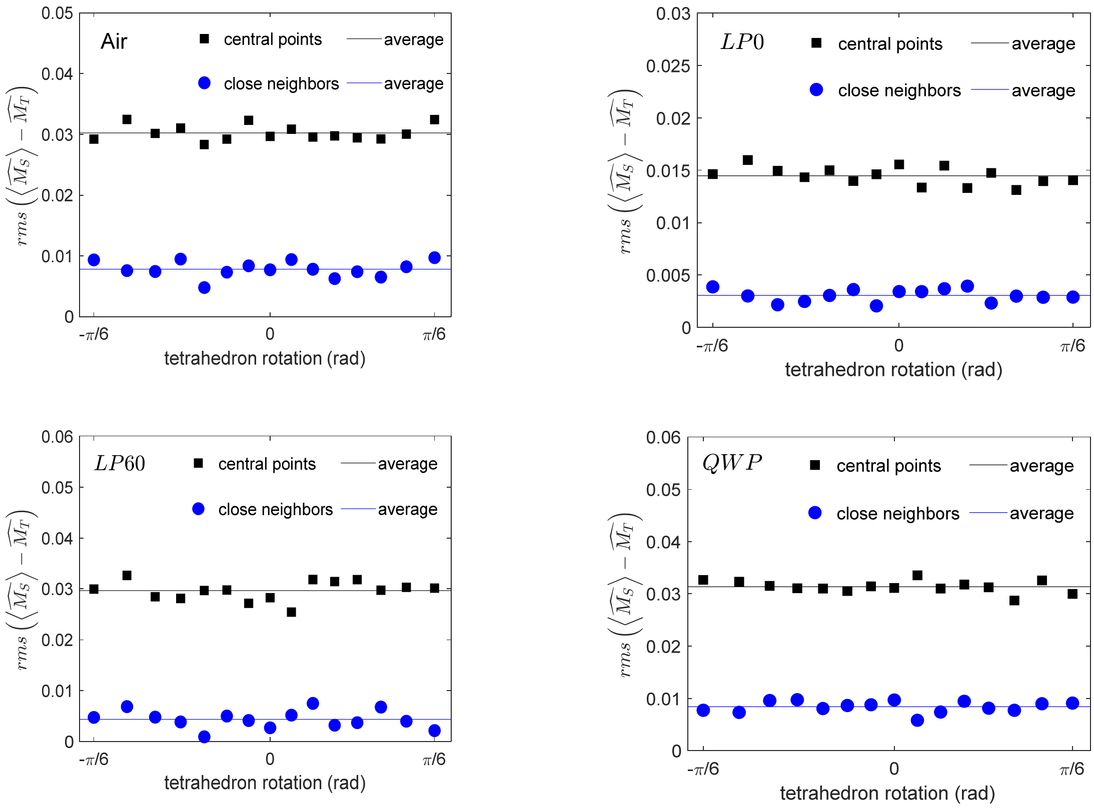

Fig. 5. Individual and mean values of the rms of differences between the Mueller matrix obtained from numerical simulation and theoretical ones, for four different ideal samples, assuming a maximum amplitude of Gaussian noise of $\varepsilon = 0.02$.

When the maximum amplitude of the added Gaussian noise (characterized by the parameter ε) is varied, the uncertainty in the errors predicted for both strategies also changes. Fig. 6 shows the average values and the error bars for seven values of ε when the sample is air: the beam does not go through any sample at all but two different Gaussian noises are added to the images in Fig. 1.b.

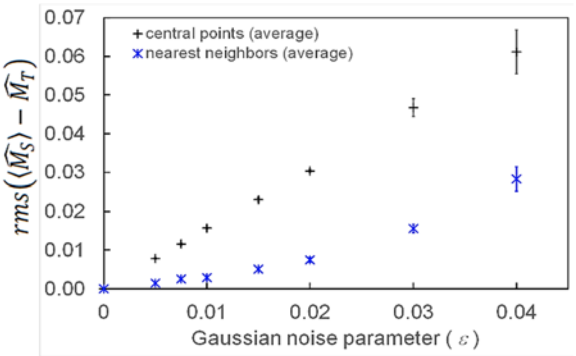

Fig. 6. Mean values of the rms of the differences between the Mueller matrix obtained from numerical simulation and the theoretical one, for air for both center points and nearest neighbors strategies. Uncertainties are indicated by vertical bars.

A comparative graph for the four samples is included in Fig. 7, for the center points strategy. The general trend is the same for all of them: the error in the determination of the elements of the Mueller matrix grows linearly as the Gaussian noise is increased. However, quantitatively, the errors for the case of a linear polarizer with horizontal transmission axis are less than a half of the other three considered samples.

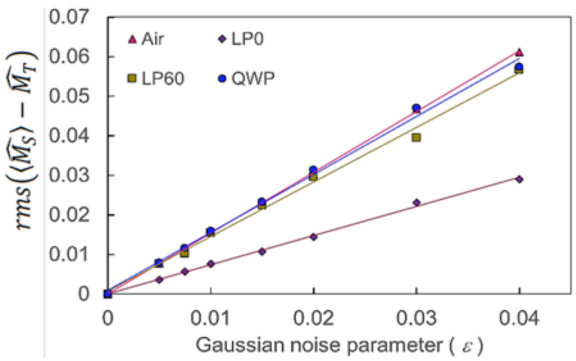

Fig. 7. Mean values of the rms of the differences between the Mueller matrix obtained from numerical simulation and the theoretical ones, for the center points strategy in the polarimetric method.

Similarly, a comparative graph for the four samples following the nearest neighbors strategy is shown in Fig. 8. In this case, the error in the determination of the elements of the Mueller matrix does not grow linearly as the Gaussian noise is increased. Calculated errors are a minimum for the case of a linear polarizer (0º), followed by the linear polarizer (60º). Mean errors in this strategy are very similar for the cases of air (no sample) and quarter wave plate linear retarder.

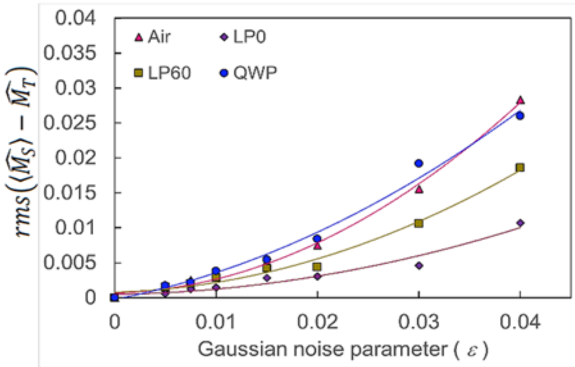

Fig. 8. Mean values of the rms of the differences between the Mueller matrix obtained from numerical simulation and the theoretical ones, for the nearest neighbors strategy in the polarimetric method.

The final goal of these simulations is to assess the differences in the mean errors that are expected using the first or the second strategy for the evaluation of $\widehat{M}$ during experimental measurement using real samples.

Fig. 9 shows the reduction in errors using the nearest neighbors strategy, as compared to the center points strategy. For all the cases, the nearest neighbors strategy is superior in terms of error reduction. A value of 80 % in error reduction can be noted for situations where the Gaussian noise parameter is $\varepsilon \leq 0.02$, for any of the samples. However, if higher levels of noise are present in the CCD images, the error reduction starts to drop steadily.

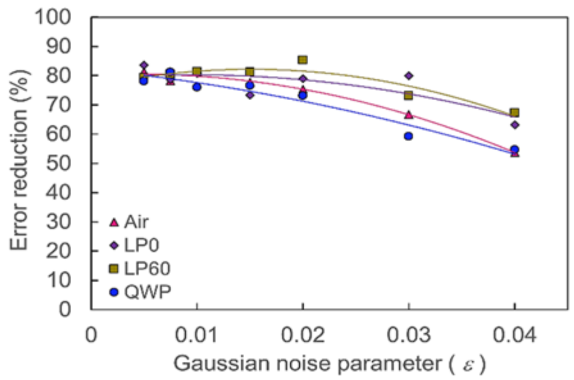

Fig. 9. Mean values of the error reduction using the nearest neighbors strategy, as compared to the center points strategy, in terms of the level of Gaussian noise in the CCD images (ε).

4. Conclusions

In the present work, it is proposed to use a full Poincaré beam together with a simple polarization state analyzer for determining the Mueller matrix of an unknown sample. Two different strategies are tested which we have called the *center points* strategy or *nearest neighbours* strategy, respectively.

From the presented simulations, it can be deduced that the information collected from the images taken with a CCD camera for six configurations of the PSA could be useful to reduce the errors due to the inaccuracy of the intensity measurement. The results obtained from these simulations will be useful for deciding a measurement strategy during the experimental development of this polarimetric method.

Acknowledgements

This work has been partially supported by Spanish Ministerio de Economía y Competitividad under project FIS2016-75147 and project PID2019 104268GB-C21.

References

[1]. G. Piquero, R. Martínez-Herrero, J. C. G. de Sande, M. Santarsiero, Synthesis and characterization of non-uniformly totally polarized light beams: tutorial, *Journal of the Optical Society of America A*, Vol. 37, Issue 4, 2020, pp. 591-605.

[2]. D. H. Goldstein, Polarized Light, Marcel Dekker, Inc., 2003.

[3]. R. A. Chipman, Polarimetry, in *Handbook of Optics*, ed., M. Bass, McGraw-Hill Companies, 1990.

[4]. J. W. Hovenier, Structure of a general pure Mueller matrix, *Applied Optics,* Vol. 33, Issue 36, 1994, pp. 8318–8324.

[5]. J. S. A. Zallat, M. P. Stoll, Optimal configurations for imaging polarimeters: impact of image noise and systematic errors, *Journal of Optics A: Pure and Applied Optics*, Vol. 8, Issue 9, 2006, pp. 807-814.

[6]. J. J. Gil, Polarimetric characterization of light and media, *The European Physical Journal Applied Physics*, Vol. 40, Issue 1, 2007, pp. 1-47.

[7]. S. Tripathi, K. C. Toussaint, Rapid Mueller matrix polarimetry based on parallelized polarization state generation and detection, *Optics Express*, Vol. 17, Issue 24, 2009, pp. 21396-21407.

[8]. G. Martínez-Ponce, C. Solano, C. Pérez-Barrios, Hybrid complete mueller polarimeter based on phase modulators, *Optics and Lasers in Engineering*, Vol. 49, Issue 6, 2011, pp.723-728.

[9]. D. M. Layden, F. G. Wood, I. A. Vitkin, Optimum selection of input polarization states in determining the sample Mueller matrix: a dual photoelastic polarimeter approach, *Optics Express*, Vol. 20, Issue 18, 2012, pp. 20466-20481.

[10]. A. Peinado, A. Lizana, A. Turpín, C. Iemmi, T. K. Kalkandjiev, J. Mompart, J. Campos, Optimization, tolerance analysis and implementation of a Stokes polarimeter based on the conical refraction phenomenon, *Optics Express,* Vol. 23, Issue 5, 2015, pp. 5636-5652.

[11]. J. C. G. de Sande, M. Santarsiero, G. Piquero, Spirally polarized beams for polarimetry measurements of deterministic and homogeneous samples, *Optics and Lasers in Engineering*, Vol. 91, 2017, pp. 97-105.

[12]. N. C. Bruce, J. M. López-Téllez, O. G. Rodríguez-Herrera, Permitted experimental errors for optimized variable-retarder Mueller-matrix polarimeters, *Optics Express*, Vol. 26, Issue 11, 2018, pp.13693-13704.

[13]. J. C. G. de Sande, G. Piquero, M. Santarsiero, Polarimetry with azimuthally polarized light, *Optics Communication*, Vol. 410, 2018, pp. 961-965.

[14]. J. del Hoyo, L. M. Sanchez-Brea, J. A. Gomez-Pedrero, High precision calibration method for a four-axis Mueller matrix polarimeter, *Optics and Lasers in Engineering*, Vol. 132, 2020, 106112, (pp. 10).

[15]. K. Singh, N. Tabebordbar, A. Forbes, A. Dudley, Digital Stokes polarimetry and its application to structured light: tutorial, *Journal of the Optical Society of America A*, Vol. 37, Issue 11, 2020, pp. C33-C44.

[16]. A. M. Beckley, T. G. Brown, M. A. Alonso, Full Poincaré beams, *Optics Express*, Vol. 18, Issue 10, 2010, pp. 10777-10785.

[17]. G. Piquero, J. Vargas-Balbuena, Non-uniformly polarized beams across their transverse profiles: An introductory study for undergraduate optics courses, *European Journal of Physics*. Vol. 25, Issue 6, 2004, pp. 793-800.

[18]. G. Piquero. L. Monroy, M. Santarsiero, M. Alonzo, J. C. de Sande, Synthesis of full Poincaré beams by means of uniaxial cristals, *Journal of Optics*, Vol. 20, Issue 6, 2018, 065602, (pp. 8).

[19]. J. C. Suárez-Bermejo, J. C. G. de Sande, M. Santarsiero, G. Piquero, Mueller matrix polarimetry using full Poincaré beams, *Optics and Lasers in Engineering*, Vol. 122, 2019, pp. 134-141.

[20]. J. C. Suárez-Bermejo, J. C. G. de Sande, M. Santarsiero, G. Piquero, Analysis of the Errors in Polarimetry with Full Poincaré Beams, in *Proceedings of the Progress in Electromagnetics Research Symposium*, *(PIERS-Rome),* 2019, pp. 2621-2627.